Available online at www.sciencedirect.com
SCIENCE DIRECT
Polymer 47 (2006) 982–990
polymer
www.elsevier.com/locate/polymer

Luminescent Nd^{3+} doped silicone–urea copolymers

Umit Demirbas [a], Adnan Kurt [a], Alphan Sennaroglu [a], Emel Yilgör [b], Iskender Yilgör [b,*]

[a] Department of Physics, Koc University, Rumelifeneri Yolu, Sariyer, Istanbul 34450, Turkey
[b] Department of Chemistry, Koc University, Rumelifeneri Yolu, Sariyer, Istanbul 34450, Turkey

Received 5 September 2005; received in revised form 16 December 2005; accepted 19 December 2005

Abstract

A simple method for the preparation of rare earth ion-doped polymers, which display luminescence, is reported. For this purpose silicone–urea copolymers were doped with $Nd(NO_3)_3 \cdot 6H_2O$. Various structural and physicochemical properties of the resultant materials were investigated. FTIR studies indicated strong interaction of Nd^{3+} ions with urea groups, but no interaction with siloxane backbone, which is expected. Absorption measurements in the visible and near infrared region were performed and the radiative decay rates and branching ratios for the meta-stable $^4F_{3/2}$ level were determined by using Judd–Ofelt theory. The samples were also excited at 800 nm and emission spectra were observed in the near infrared at 905, 1059, and 1331 nm. In Nd^{3+} doped silicone–urea systems the highest emission cross section at 1059 nm was determined to be 60.7×10^{-21} cm^2. Spectroscopic parameters determined in this study suggest that Nd^{3+} doped silicone–urea copolymers are promising candidates for the development of fiber lasers or amplifiers near 1.06 and 1.3 μm.

Keywords: Metal–ion doped polymers; Luminescent polymers; Polymers for fiber optics

1. Introduction

There has been a growing interest in the development of rare-earth ion (RE) doped polymers for numerous applications in fiber–optic communications systems, fiber laser development, and optical sensing [1–15]. Polymer-based alternatives to existing RE doped glasses offer many advantages, which include; (i) a wide selection of host polymers with different mechanical properties, ranging from elastomers to rigid and tough thermoplastics, (ii) possibility of doping large amounts of RE into polymers without clustering, (iii) ease of sample preparation, and (iv) reduced costs in mass production. Possibility of the incorporation of a wide selection of RE ions into the host polymers provide opportunities in the production of absorption and emission bands covering selected ranges of the electromagnetic spectrum [10]. In spite of these advantages, polymers may have two major drawbacks when used as hosts for rare earth ions. These are; (i) limited solubility of RE ion in the host polymer, which is critical in order to obtain a homogeneous distribution of RE in the polymer matrix, and a thermodynamically stable system, and (ii) possible interaction (vibrational coupling) between (C–H) and (if present, O–H) groups in the polymer and RE, resulting in non-radiative deactivation or quenching [8,13]. Solubility problem can be circumvented by either designing host polymers with specific functional groups along the backbone [13,16] or by using organic ligands (or surfactants) that can interact with RE ions through complex formation and that are also miscible with the host polymer [13,17,18]. The first approach is fairly difficult since it generally requires specialty monomers and strict control of functional group distribution along the polymer backbone during polymerization. Use of organic ligands or surfactants is a much simpler approach. For this purpose organic surfactants with carboxylic acid [8,17], amine [18], acetylacetonate [4,10] and other types of functional groups [4,13] and linear or dendritic [17] backbones have been successfully utilized. Strong interaction (or complex formation) between RE ion and the surfactant forms a protective cage [8,13,17] around the RE ion. As an added benefit, this reduces the possibility of vibrational coupling between (C–H) bonds in the host polymer and the RE ion or the possibility of non-radiative deactivation or quenching.

We have been investigating the synthesis, characterization and structure–property behavior of polydimethylsiloxane–urea (PDMS–urea) copolymers with a wide range of compositions for over two decades [19–22]. Due to substantial differences between the solubility parameters of PDMS (15.5 $J^{1/2}$ cm$^{-3/2}$) and urea (45.6 $J^{1/2}$ cm$^{-3/2}$) [23], silicone–urea copolymers

* Corresponding author. Tel.: +90 212 338 1418; fax: +90 212 338 1559.
E-mail address: iyilgor@ku.edu.tr (I. Yilgör).

0032-3861/$ - see front matter © 2006 Elsevier Ltd. All rights reserved.
doi:10.1016/j.polymer.2005.12.076

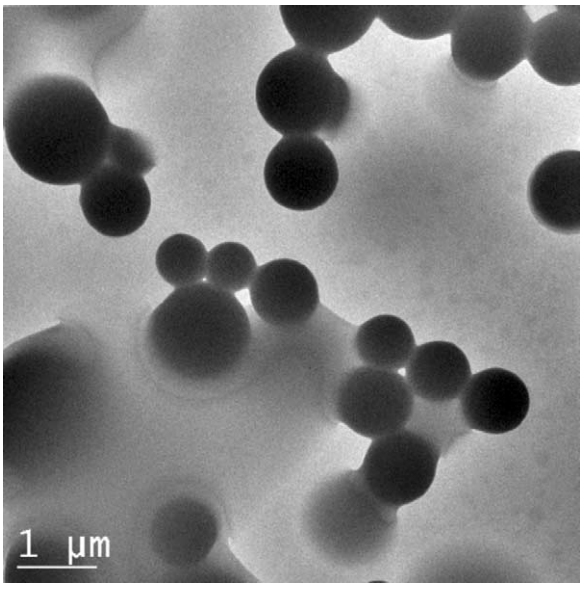

Fig. 1. TEM photomicrograph of a cobalt(II) chloride doped silicone–urea copolymer containing 18% by weight urea hard segments.

display well separated microphase morphologies [20,22], where urea domains are distributed in a continuous PDMS matrix. This can clearly be seen in Fig. 1, where a TEM photomicrograph of cobalt(II) chloride doped PDMS–urea copolymer ([$CoCl_2$]/[urea] = 0.50) with a urea hard segment content of 18% by weight is provided. We believe this TEM picture represents the first direct observation of well phase separated microphase morphology in PDMS–urea copolymers, where a transition metal salt, cobalt(II) chloride, is used as a staining agent for urea domains, since it selectively interacts with polar urea groups but not with PDMS. Spherical polyurea domains with diameters between 500 and 1000 nm are clearly visible in the continuous PDMS matrix. Similar morphologies have also been observed by others using AFM [24]. In our earlier studies, through quantum mechanical calculations and related laboratory experiments, we also demonstrated that when PDMS–urea copolymers are doped with $CoCl_2$, as expected, polar Co^{2+} ions preferentially migrate to the urea domains [25]. In the present study, we report a simple method for the preparation of Nd^{3+}-doped, luminescent silicone–urea copolymers and spectroscopic characteristics of these novel systems.

2. Experimental

2.1. Materials

α,ω-Aminopropyl terminated polydimethylsiloxane (PDMS) oligomers with number average molecular weights $\langle M_n \rangle$ of 2500 and 3200 g mol^{-1} were obtained from Wacker-Chemie, Munich, Germany. α,ω-Amine terminated poly(ethylene oxide) (PEO) with $\langle M_n \rangle$ of 900 g mol^{-1} was provided by Huntsman. Bis(4-isocyanatocyclohexyl)methane (HMDI) with a purity greater than 99.5% was supplied by Bayer AG. 2-Methyl-1,5-diaminopentane (DY) was kindly supplied by DuPont. Neodymium(III) nitrate hexahydrate ($Nd(NO_3)_3 \cdot 6H_2O$) (99.9%) was a product of Aldrich. Chromatographic grade reaction solvents, tetrahydrofuran (THF) and isopropanol (IPA) were obtained form Carlo Erba and were used without further purification.

2.2. Polymer synthesis

Silicone–urea and polyether modified silicone–urea copolymers were synthesized in three-neck, round bottom, Pyrex flasks, fitted with an overhead stirrer, addition funnel and nitrogen inlet. Reactions were carried out at room temperature using the two-step prepolymer method. Prepolymer was obtained by the dropwise addition of a solution of the amine terminated PDMS (in THF) into the reactor containing HMDI (also dissolved in THF). In polyether modified copolymer, prepolymer is obtained by the subsequent, dropwise addition of PDMS and PEO into HMDI solution in the reactor. For chain extension, a stoichiometric amount of diamine (DY) was dissolved in IPA and added dropwise into the reactor, through an addition funnel. Detailed procedures for copolymer syntheses are provided elsewhere [21,22]. FT-IR was used to determine the completion of the reaction by monitoring the disappearance of the strong isocyanate peak at 2270 cm^{-1}. Chemical compositions of the silicone–urea copolymers are provided on Table 1.

2.3. Preparation of $Nd(NO_3)_3 \cdot 6H_2O$ doped films

Depending on the level of Nd^{3+} ion incorporation, a calculated amount of $Nd(NO_3)_3 \cdot 6H_2O$ was dissolved in THF in a beaker. Then it is mixed with the desired amount of silicone–urea copolymer solution in THF or THF/IPA. Clear and homogeneous mixtures obtained were poured into a Teflon mold and the solvent was evaporated at room temperature, overnight. To prevent decomposition of nitrate groups and oxidation of polymer backbone, doped films were dried in a vacuum oven at room temperature until constant weight and kept in sealed polyethylene bags until further use. Compositions of the $Nd(NO_3)_3$ doped silicone–urea copolymers are provided on Table 2.

Table 1
Chemical compositions of silicone–urea copolymers

Polymer Code	PDMS $\langle M_n \rangle$ (g mol^{-1})	PEO $\langle M_n \rangle$ (g mol^{-1})	PDMS (wt%)	PEO (wt%)	HMDI (wt%)	DY (wt%)	HS (wt%)
PSU-1	3200	–	92.4	–	7.6	–	7.6
PSU-2	2500	900	50.0	20.0	24.2	5.8	30.0

Table 2
Compositions of the $Nd(NO_3)_3$ doped silicone–urea copolymers

Polymer code	Polymer (g)	$Nd(NO_3)_3 \cdot 6H_2O$ (g)	$[Nd^{3+}]$/[urea]	Nd^{3+}(wt%)
PSU-1-7	8.00	2.00	1.0	6.58
PSU-2-18	4.57	5.43	1.5	17.9

2.4. Spectroscopic characterization

FTIR spectroscopy was used to investigate the interaction between silicone–urea copolymers and the $Nd(NO_3)_3 \cdot 6H_2O$. FTIR scans were collected on thin films cast on KBr discs from THF solution, on a Nicolet Impact 400D FTIR spectrometer. Spectra were collected using 20 scans with a resolution of 2 cm^{-1}.

UV–visible absorption spectra of the polymers were measured on a Shimadzu model 3101 PC, UV–VIS–NIR spectrometer between 300 and 900 nm. During the measurements polymer films with a thickness of 1–2 mm were used.

Emission intensity measurements were performed by using the experimental setup sketched in Fig. 2. A tunable Ti:Sapphire laser was used as the pump source. It was tuned to the absorption band of the Nd^{3+} ion near 799 nm and produced 50-ns-long pulses at a pulse repetition rate of 1 kHz. The average output power of the laser was about 50 mW. In the luminescence measurements, the pump beam was focused inside the polymer samples with a converging lens (L1, focal length = 8 cm). The emitted fluorescence was collected with a concave gold mirror and imaged to the entrance slit of a 0.5 m Czerny–Turner type monochromator (CVI, model DK 480), after passing through a high-pass optical filter (F) that blocked the pump radiation. The fluorescence signal was detected with a PbS detector (DET) and amplified by using a preamplifier (PA) and a lock-in amplifier (LA, Stanford Research, model SR 830).

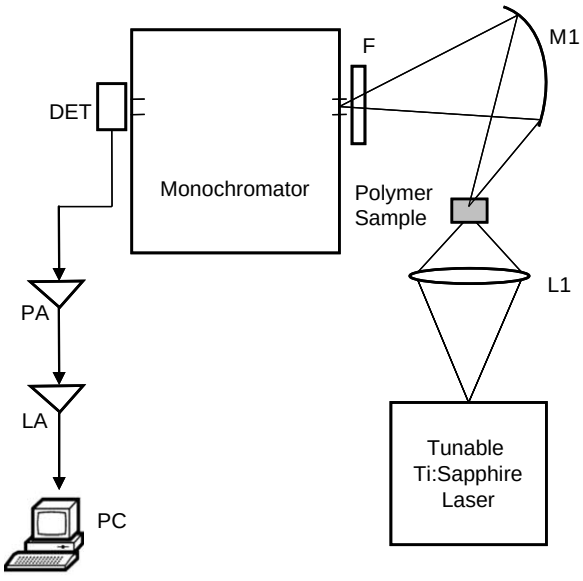

Fig. 2. Experimental setup used in the luminescence measurements.

3. Results and discussion

3.1. FTIR spectroscopy

Rare-earth ion doped polymeric systems have received interest as versatile materials for optical amplifiers [8,13]. Compared to inorganic glasses, polymers offer several important advantages, such as ease of preparation and incorporation of large concentrations of dopants. Silicone–urea copolymers are interesting materials since they are composed of alternating sequences of highly non-polar PDMS and highly polar urea units in their backbones. Substantial differences in the solubility parameters of PDMS and urea results in well separated microphase morphologies [20,22]. Similarly, in PEO modified PDMS–urea copolymers good phase separation is observed. When doped with transition metal salts, polar urea domains act as hosts for highly polar ions, whereas no interaction with the PDMS matrix is expected. This selective interaction between the urea groups and the transition metal ions was the main reason for our choice of silicone–urea copolymers as the host resin for Nd^{3+} doping in this study. This can clearly be seen in the FTIR spectra provided in Fig. 3(a)–(c) for neat $Nd(NO_3)_3 \cdot 6H_2O$, undoped silicone–urea (PSU-1) and Nd^{3+} doped silicone–urea (PSU-1-7) copolymers. FTIR spectrum of $Nd(NO_3)_3 \cdot 6H_2O$ shows a very broad hydroxy peak between 3000 and 3700 cm^{-1}, and two strong N=O stretching peaks at 1467 (anti) and 1331 cm^{-1} (sym). The bands at 1331, 1467 and 1642 cm^{-1} indicate that the $[NO_3]^-$ groups are acting both as monodentate and chelating bidentate ligands towards the central Nd atom. Fig. 3(b) shows the 900–1800 cm^{-1} region of the FTIR spectra, which covers the carbonyl (C=O) (amide I and amide II) (1500–1700 cm^{-1}) and siloxane (Si–O–Si) (950–1200 cm^{-1}) absorption regions. In this region undoped PSU-1 shows two very strong carbonyl absorption bands with peak maxima at 1631 cm^{-1} (strongly hydrogen bonded C=O, amide I) and 1567 cm^{-1} (amide II), a strong and sharp peak at 1262 cm^{-1} (symmetric CH_3 deformation in PDMS) and a strong doublet with maxima at 1024 and 1095 cm^{-1} (asymmetric Si–O–Si stretching). As expected, the carbonyl region of the FTIR spectrum of Nd^{3+} doped copolymer (PSU-1-7) is quite different than that of undoped PSU-1. Well-defined doublet of PSU-1 is replaced with a very broad peak extending from 1700 to 1550 cm^{-1}, clearly indicating very strong interaction between Nd^{3+} and the urea groups. In Nd-doped PSU two new, strong absorption bands centered around 1470 and 1323 cm^{-1} are also observed, which are due to antisymmetric and symmetric N=O stretching, respectively. Interestingly there is no change in the peaks originating from the PDMS in the system, which are at 1262 cm^{-1} (symmetric CH_3 deformation in PDMS) and the strong doublet with maxima at 1095 and 1024 cm^{-1} due to asymmetric Si–O–Si stretching. These results clearly indicate that there is no interaction between Nd^{3+} and the PDMS as expected and RE ions are mainly distributed in the urea domains. Further confirmation of the interaction between Nd^{3+} and urea groups comes from Fig. 3(c), where 2750–3850 region of the FTIR

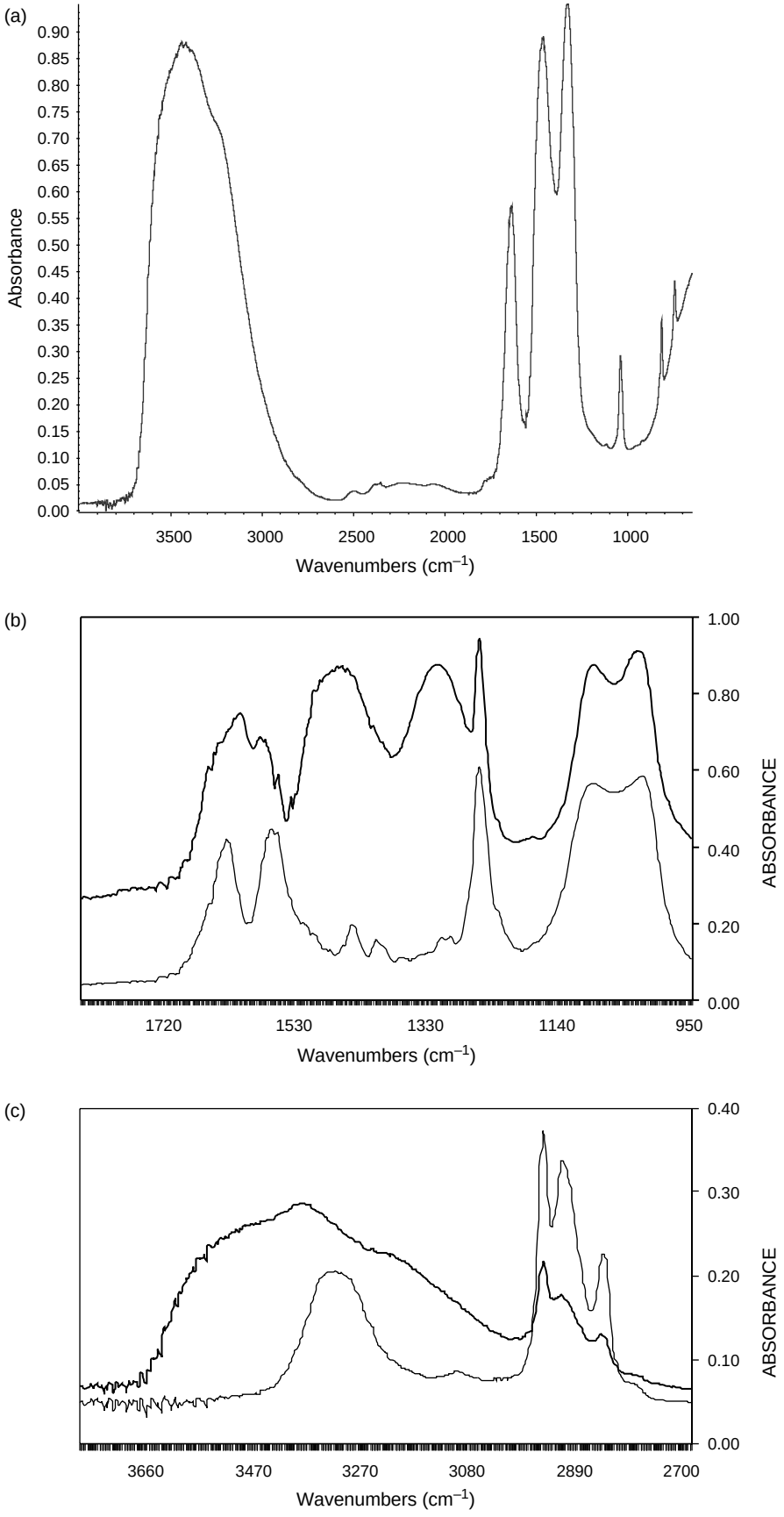

Fig. 3. (a) FTIR spectra of $Nd(NO_3)_3 \cdot 6H_2O$; (b) comparative FTIR spectra of PSU-1 (—) and PSU-1-7 (▬) in amide-I and amide-II regions 950–1850 cm^{-1}; (c) comparative FTIR spectra of PSU-1 (—) and PSU-1-7 (▬) in 2750–3850 cm^{-1}.

spectra are reproduced. It is important to note that the shape or positions of the aliphatic C–H stretching bands in PDMS at 2963, 2928 and 2854 cm^{-1} are unchanged, indicating no interaction with Nd^{3+}. On the other hand, well-defined hydrogen bonded N–H peak centered at 3335 cm^{-1} in PSU-1 has been replaced with a very broad absorption band in $Nd(NO_3)_3 \cdot 6H_2O$ doped material, which extends from 3000 to 3700 cm^{-1}, with a peak at 3400 cm^{-1} and a shoulder at 3233 cm^{-1}. These results show strong interaction between Nd^{3+} and the urea groups [25–28].

3.2. Density and refractive index measurements

The densities of PSU-1-7 and PSU-2-18 were determined by using a picnometer and found to be 1.02 ± 0.02, and 1.40 ± 0.02 g cm^{-3}, respectively. Using the densities and the weight ratio of Nd^{3+} ions in the copolymer host, we estimate the Nd^{3+} ion concentrations to be $2.80 \pm 0.05 \times 10^{+20}$ and $10.46 \pm 0.15 \times 10^{+20}$ cm^{-3} for PSU-1-7 and PSU-2-18, respectively.

Refractive index measurements were all done at 25 °C with visible light using an Abbe refractometer. Refractive indices of the undoped PSU-1 and PSU-2 films were measured to be 1.425 ± 0.002 and 1.448 ± 0.002, respectively. After doping with Nd^{3+} the refractive indices of the samples increased to 1.482 ± 0.002 (PSU-1-7) and 1.503 ± 0.002 (PSU-2-18). The density and refractive index values were used in the Judd–Ofelt analysis described below to determine the radiative emission strengths of the Nd^{3+} ion in the polymer hosts.

3.3. Judd–Ofelt analysis

The measured absorption spectrum of Nd-doped PSU-1-7 sample is shown in Fig. 4. The film thickness and dopant concentration were 1.98 mm, and $2.80 \times 10^{+20}$ cm^{-3}, respectively, giving an estimated absorption coefficient of 5.68 cm^{-1} and corresponding absorption cross section of 2.03×10^{-20} cm^2 at the wavelength of 799 nm. Similarly, the

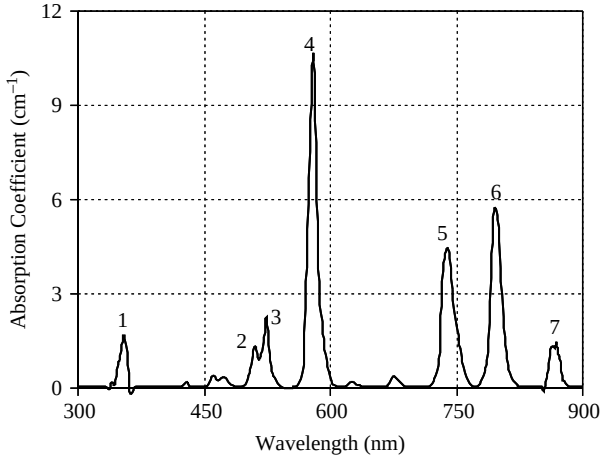

Fig. 4. Measured absorption spectrum of Nd-doped PSU-1-7 with an estimated concentration and sample thickness of $2.8 \times 10^{+20}$ cm^{-3} and 1.98 mm, respectively.

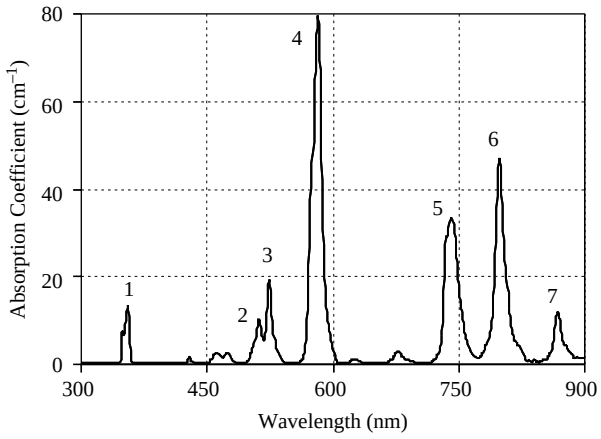

Fig. 5. Measured absorption spectrum of Nd-doped PSU-2-18 with an estimated concentration and sample thickness of $10.3 \times 10^{+20}$ cm^{-3} and 1.12 mm, respectively.

absorption spectrum of the Nd-doped PSU-2-18 sample (concentration = $10.46 \times 10^{+20}$ cm^{-3}, sample thickness = 1.12 mm) is displayed in Fig. 5. In this case, the estimated absorption cross section at 799 nm was 4.40×10^{-20} cm^2. Table 3 further lists the cross sections for the strongest absorption bands recorded between 300 and 900 nm. Note that the absorption peak positions of PSU-1-7 and PSU-2-18 are almost the same. Also, the measured absorption spectra of Nd^{3+} ion do not differ significantly in comparison with other Nd^{3+} doped polymers, and the observed peak positions are approximately the same [11,29]. Comparing with Nd:YAG, most of the absorption peaks shifted slightly (~5 nm) to shorter wavelengths [30]. However, the relative intensities of the absorption peaks differ considerably in different hosts [2,12,15,30], since it is affected by the coordination structure of the Nd^{3+} ion in the host. As an example, in Nd:YAG, the strongest absorption line is due to the $^4I_{9/2} \rightarrow {}^4F_{5/2} + {}^2H_{9/2}$ transition [30], however, in our case $^4I_{9/2} \rightarrow {}^4G_{5/2} + {}^2G_{7/2}$ is the strongest line in the absorption spectrum. The relative intensities of the absorption bands were also different between PSU-1-7 and PSU-2-18. In particular, the absorption cross section of PSU-2-18 is approximately twice as large as that for PSU-1-7 (Table 3). The peak absorption cross section observed in PSU-2-18 at 582 nm (7.59×10^{-20} cm^2, due to the $^4I_{9/2} \rightarrow {}^4G_{5/2} + {}^2G_{7/2}$ transition) is comparable with the values

Table 3
Position of the absorption peaks, the corresponding electronic transition, and the estimated peak cross section of the absorption bands of Nd-doped PSU-1-7 and Nd-doped PSU-2-18 between 300 and 900 nm

λ (nm)	Transition $^4I_{9/2} \rightarrow$	Peak #	σ ($\times 10^{-20}$ cm^2)	
			PSU-1-7	PSU-2-18
355	$^4D_{3/2} + {}^2I_{11/2} + {}^4D_{5/2} + {}^4D_{1/2} + {}^2L_{15/2}$	1	0.58	1.25
512	$^2K_{13/2} + {}^4G_{9/2}$	2	0.55	0.92
525	$^4G_{7/2}$	3	0.78	1.81
582	$^4G_{5/2} + {}^2G_{7/2}$	4	3.78	7.59
741	$^4F_{7/2} + {}^4S_{3/2}$	5	1.58	3.17
799	$^4F_{5/2} + {}^2H_{9/2}$	6	2.03	4.39
868	$^4F_{3/2}$	7	0.51	1.11

reported for other polymer hosts [2,11]. With the possibility of high active ion doping levels (17.9 wt% Nd^{3+} in PSU-2-18) in our synthesis technique, we obtained absorption coefficients up to 79.75 cm^{-1} at 582 nm. This is a good indication of the effectiveness of silicone–urea copolymers as hosts for RE ions in optical applications.

The Judd–Ofelt theory [31,32] was further used to analyze the absorption spectra and determine the radiative decay rates as well as the emission cross sections. The spectral intensity f_{exp}, also known as the integrated absorbance, was determined experimentally for the 10 strongest absorption bands (between 345 and 910 nm) by using

$$f_{exp} = \int_{band} \mu(\lambda)d\lambda. \quad (1)$$

Here, λ is the wavelength and $\mu(\lambda)$ is the absorption coefficient given by

$$\mu(\lambda) = \frac{\ln(I_0/I)}{l}. \quad (2)$$

In Eq. (2), I_0 and I are the respective incident and transmitted intensities, and l is the sample thickness. For lanthanide (Ln^{+3}) ion-doped materials, experimentally measured oscillator strengths (f_{exp}) can be attributed to, electric dipole, magnetic dipole, and electric quadrupole transitions [33]. Earlier studies on Ln^{+3} ion doped materials [34,35] showed that electric quadrupole oscillator strengths are much smaller than those for electric dipole and magnetic dipole interactions (in the order of $\sim 10^{-11}$ [14,36], roughly four orders of magnitude smaller than electric dipole strength [4,37]). Magnetic dipole oscillator strengths are not host dependent, and tabulated values in the literature [38] are two orders of magnitude smaller than those for electric dipole transitions [4]. Hence, contributions of electric quadrupole and magnetic dipole transitions were neglected as was done in previous studies [11,39].

According to Judd–Ofelt theory, the spectral intensity for an electric dipole transition from the ground state (SLJ) to the excited state ($S'L'J'$) is given by,

$$f_{cal}(J,J') = \frac{8\pi^3 e^2}{3ch}\frac{(n^2+2)^2}{9n}\frac{\bar{\lambda}}{(2J+1)}N_0 \times \sum_{t=2,4,6} \Omega_t |\langle SLJ\|U^{(t)}\|S'L'J'\rangle|^2. \quad (3)$$

Above, $\bar{\lambda}$ is the mean wavelength for the absorption band (or bands in the case of overlapping Stark manifolds), n is the refractive index, c is the speed of light, h is Planck's constant, J is the total angular momentum quantum number of the ground state, $U^{(t)}$ are the doubly reduced matrix elements of the unit tensor operator of rank t, Ω_t are the Judd–Ofelt intensity parameters, and N_0 is the concentration of the Nd^{3+} ions in the polymer sample. Since the reduced matrix elements $U^{(t)}$ are not strongly host-dependent [39], we used the values reported for $Lu_3Sc_2GaO_{12}$ [35,40]. For the overlapping Stark manifolds, the sum of all the corresponding squared matrix elements were taken [35]. The three Judd–Ofelt intensity parameters Ω_2, Ω_4, and Ω_6 were determined by doing a least squares fitting of $f_{cal}(J,J')$ with f_{exp}.

The radiative lifetime τ_R for the ith excited state is given by

$$\frac{1}{\tau_R(i)} = \sum_j A(i,j) = W_R, \quad (4)$$

where $A(i,j)$ is the spontaneous emission probability for the transition from the ith state to the jth state and summation is carried over all of the lower states (j) to determine the total spontaneous fluorescence probability, W_R. The spontaneous emission probability $A(J,J')$ for an $SLJ \rightarrow S'L'J'$ electric-dipole transition can be calculated from

$$A(J,J') = \frac{64\pi^4 e^2}{3h(2J+1)}\frac{n(n^2+2)^2\bar{\nu}^3}{9}\sum_{t=2,4,6}\Omega_t|\langle SLJ\|U^{(t)}\|S'L'J'\rangle|^2 = \frac{64\pi^4 e^2}{3h(2J+1)}\frac{n(n^2+2)^2\bar{\nu}^3}{9}S^{ed}(J,J'), \quad (5)$$

where, $\bar{\nu}$ is the mean wave number of the transition. By using the matrix elements given in [35] for the Nd^{3+} ion, for the meta-stable $^4F_{3/2}$ level, the expressions for S^{ed} appearing in Eq. (5) becomes

$$S^{ed}[^4F_{3/2} \rightarrow {}^4I_{15/2}] = 0.0288\,\Omega_6 \quad (6)$$

$$S^{ed}[^4F_{3/2} \rightarrow {}^4I_{13/2}] = 0.0285\,\Omega_6 \quad (7)$$

$$S^{ed}[^4F_{3/2} \rightarrow {}^4I_{11/2}] = 0.1136\,\Omega_4 + 0.4104\,\Omega_6 \quad (8)$$

and

$$S^{ed}[^4F_{3/2} \rightarrow {}^4I_{9/2}] = 0.2293\,\Omega_4 + 0.0548\,\Omega_6 \quad (9)$$

for the emission bands at 1818, 1331, 1059 and 905 nm, respectively. Note that spontaneous emission probability for the $^4F_{3/2} \rightarrow {}^4I_{15/2}$ is negligible with respect to others. The best-fit values of the Judd–Ofelt intensity parameters were used to calculate the expressions for S^{ed} in Eqs. (6)–(8) and the radiative lifetimes.

Summary of the Judd–Ofelt analysis results is shown in Table 4. The measured and calculated transition strengths for the two copolymer samples are shown at the top part of Table 4. The root-mean square errors σ_{rms} were calculated in the usual way using

$$\sigma_{rms} = \sqrt{\frac{\sum (f_{cal} - f_{exp})^2}{q-p}} \quad (10)$$

where q is the number of absorption bands included in the calculation and p is the number of parameters determined ($q=10$, and $p=3$ in our case) [35]. Calculated root-mean square errors for PSU-1-7 (0.43×10^{-6}) and PSU-2-18 (3.02×10^{-6}) are comparable with the values in previous studies [4,14,30,41]. The good agreement between experimental and

Table 4
Measured and calculated spectral intensities, best-fit Judd–Ofelt intensity parameters Ω_2, Ω_4 and Ω_6, the spectroscopic quality parameter, and the radiative lifetime ($^4F_{3/2}$ level) for Nd^{3+}-doped PSU-1-7 and PSU-2-18

Excited states $^4I_{9/2}\rightarrow$	Wavelength range (nm)	PSU-1-7		PSU-2-18	
		f_{exp} ($\times10^{-6}$)	f_{cal} ($\times10^{-6}$)	f_{exp} ($\times10^{-6}$)	f_{cal} ($\times10^{-6}$)
$^4D_{3/2}+{}^2I_{11/2}+{}^4D_{5/2}+{}^4D_{1/2}+{}^2L_{15/2}$	335–365	2.19	1.90	12.33	16.02
$^2P_{1/2}+{}^2D_{5/2}$	425–440	0.16	0.14	1.22	1.19
$^2K_{15/2}+{}^2D_{3/2}+{}^2G_{9/2}+{}^4G_{11/2}$	450–490	0.66	0.46	4.57	3.85
$^2K_{13/2}+{}^4G_{9/2}+{}^4G_{7/2}$	490–545	3.56	2.68	26.99	21.98
$^2G_{7/2}+{}^4G_{5/2}$	555–605	14.41	14.46	114.35	114.68
$^2H_{11/2}$	610–645	0.14	0.12	0.91	1.04
$^4F_{9/2}$	655–700	0.36	0.54	3.87	4.46
$^4F_{7/2}+{}^4S_{3/2}$	715–770	8.63	8.56	67.71	70.89
$^4F_{5/2}+{}^2H_{9/2}$	770–830	8.48	8.64	75.12	71.69
$^4F_{3/2}$	845–910	1.84	2.40	18.60	20.12
σ_{rms} ($\times10^{-6}$)		0.43		3.02	
J–O intensity parameters		PSU-1-7		PSU-2-18	
Ω_2 ($\times10^{-20}$ cm^2)		5.54		11.37	
Ω_4 ($\times10^{-20}$ cm^2)		2.23		4.95	
Ω_6 ($\times10^{-20}$ cm^2)		4.77		10.41	
X_{ND} ($^4F_{3/2}$) $=\Omega_4/\Omega_6$		0.47		0.48	
$\tau_R=(1/W_R)$ (μs)		541		236	

calculated transitions strengths show that the assignment of the electronic transitions for the absorption bands are correct, and the contributions from electric quadrupole and magnetic dipole transitions are very small as assumed.

Bottom part of Table 4 lists the best-fit values of the Judd–Ofelt intensity parameters, and the radiative lifetime for the $^4F_{3/2}$ level. We also included the spectroscopic quality parameter (defined as Ω_4/Ω_6), which is the only parameter that affects the inter-manifold transition probabilities for the $^4F_{3/2}$ level, since the elements of $U^{(2)}$ are all zero (the doubly reduced matrix elements of the unit tensor operator of rank 2 for $^4F_{3/2}$ transitions) (Eqs. (6)–(9)) [35]. It is well known that the Judd–Ofelt intensity parameters are related to the nature of the chemical bonding and the coordination structure of the rare earth ions. Previous studies reported that, lanthanide ions in a symmetric crystal matrix has low Ω_2 values due to the domination of magnetic dipole transition over electric dipole transition [13–15]. Both PSU-1-7 and PSU-2-18 samples have relatively large Ω_2 values, indicating low local symmetry for the Nd^{3+} ions in the matrix. Calculated radiative lifetimes for the $^4F_{3/2}$ meta-stable level showed that PSU-1-7, has roughly two times longer radiative lifetime. Reported values for radiative lifetimes in the literature are similar [4,15].

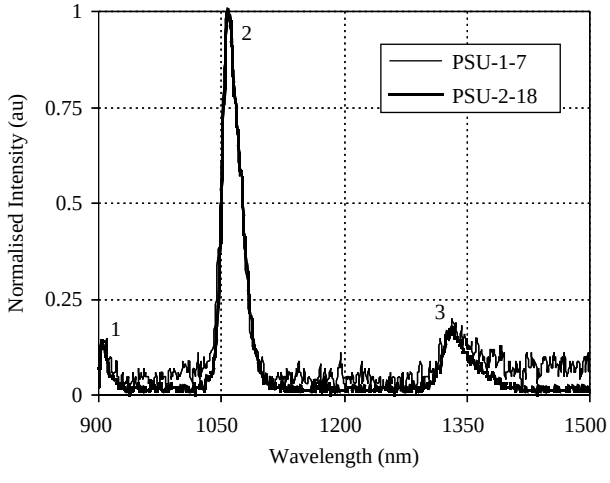

Fig. 6. Measured luminescence bands of Nd-doped PSU-1-7 and PSU-2-18 between 900 and 1500 nm.

3.4. Emission spectroscopy

The measured variation of the detected fluorescence intensity as a function of wavelength is shown in Fig. 6. Note that the relative intensity of the 1331 nm band with respect to the 1064 nm band is comparable to those in other Nd-containing hosts while the intensity of the 905 nm line is somewhat lower in our samples [2,14]. Table 5 further lists the relative strengths of these luminescence bands in the two hosts. In order to compare the two copolymer hosts, the fluorescence efficiency η_F at 1059 nm, defined as

$$\eta_F = \frac{I_{1059}}{P_{abs}}, \tag{11}$$

Table 5
Relative intensities of the dominant emission bands of Nd-doped PSU-1-7 and PSU-2-18 between 900 and 1500 nm (the data were not corrected for the detector and monochromator response)

λ (nm)	Transition	Peak #	I (a.u.)
905	$^4F_{3/2}\rightarrow{}^4I_{9/2}$	1	0.14
1059	$^4F_{3/2}\rightarrow{}^4I_{11/2}$	2	1
1331	$^4F_{3/2}\rightarrow{}^4I_{13/2}$	3	0.17

Table 6
Fluorescence branching ratios and the stimulated emission cross-sections of $^4F_{3/2} \rightarrow {}^4I_{13/2}$ (1331 nm), $^4F_{3/2} \rightarrow {}^4I_{11/2}$ (1059 nm) and $^4F_{3/2} \rightarrow {}^4I_{9/2}$ (905 nm) transitions for PSU-1-7 and PSU-2-18 polymer samples

Polymer sample	$^4F_{3/2} \rightarrow {}^4I_{13/2}$		$^4F_{3/2} \rightarrow {}^4I_{11/2}$		$^4F_{3/2} \rightarrow {}^4I_{9/2}$	
	β	σ_{se} ($\times 10^{-21}$ cm^2)	β	σ_{se} ($\times 10^{-21}$ cm^2)	β	σ_{se} ($\times 10^{-21}$ cm^2)
PSU-1-7	0.122	11.89	0.534	27.33	0.338	15.10
PSU-2-18	0.121	26.35	0.532	60.70	0.341	33.86

(I_{1059}, measured fluorescence intensity at 1059 nm and P_{abs}, absorbed pump power at the excitation wavelength, 799 nm) was also measured. The fluorescence efficiency of Nd-doped PSU-2-18 copolymer was found to be about two times larger than that in Nd-doped PSU-1-7 copolymer.

Luminescence data of the neodymium-doped samples were also used to determine the emission cross sections at 1331, 1059 and 905 nm. For an electric-dipole transition between the states (SLJ) and ($S'L'J'$), the peak stimulated emission cross section σ_{se} is given by

$$\sigma_{se} = \frac{\lambda_p^4}{8\pi c n^2 \Delta\lambda} A(J,J') \tag{12}$$

where λ_p is the peak emission wavelength, n is the refractive index of the host, $\Delta\lambda$ is the width of the luminescence band, and $A(J,J')$ is the spontaneous emission probability given in Eq. (5) [42]. From the experimentally measured emission data, we determined the widths of the luminescence bands as 14 nm (905 nm emission), 27 nm (1059 nm emission), and 35 nm (1331 nm emission). Table 6 shows the calculated fluorescence branching ratios and the stimulated emission cross sections of $^4F_{3/2} \rightarrow {}^4I_{13/2}$ (1331 nm), $^4F_{3/2} \rightarrow {}^4I_{11/2}$ (1059 nm) and $^4F_{3/2} \rightarrow {}^4I_{9/2}$ (905 nm) transitions for PSU-1-7 and PSU-2-18 polymer samples. The emission cross section value of PSU-2-18 for the $^4F_{3/2} \rightarrow {}^4I_{11/2}$ transition is 2.2 times larger than PSU-1-7, which is in good agreement with the measured relative fluorescence efficiency. The peak emission cross section value of PSU-2-18 obtained in this study for the $^4F_{3/2} \rightarrow {}^4I_{11/2}$ transition (60.7×10^{-21} cm^2) is higher than some of the previously reported Nd^{+3} doped polymers [11,14,15], and glasses [29,39,43,44]. Calculated fluorescence branching ratios for the meta-stable $^4F_{3/2}$ level are similar to the values reported in the literature [14,41,44], and the $^4F_{3/2} \rightarrow {}^4I_{11/2}$ (1059 nm) transition has the highest branching ratio, in agreement with the measured fluorescence intensities. Comparing with previous studies [10,14,15,39,44], PSU-1-7 and PSU-2-18 have low spectroscopic quality parameters, which decreases the branching ratio for the $^4F_{3/2} \rightarrow {}^4I_{9/2}$ (905 nm) transition, enhancing the 1059 and 1331 nm transitions. The results indicate that the Nd-doped silicone–urea copolymer hosts are promising candidates for the development of fiber lasers or amplifiers near 1.06 and 1.3 μm.

4. Conclusions

Preparation and various characteristics of rare earth ion (Nd^{3+}) doped, luminescent silicone–urea copolymers were discussed. Due to substantial solubility difference between PDMS and urea groups, silicone–urea copolymers display very good phase separation. It was demonstrated that Nd^{3+} ions interact only with highly polar urea groups but not with non-polar PDMS. Optical characteristics of two different Nd^{3+} doped silicone–urea copolymers (PSU-1-7 and PSU-2-18) were investigated. Absorption and emission measurements were analyzed with Judd–Ofelt theory. Studies show that PSU-2-18 sample has larger absorption cross section, emission cross-section and fluorescence efficiency than PSU-1-7 sample. Measured and calculated optical parameters of the PSU-2-18 sample show that Nd^{3+} doped silicone–urea copolymer are promising candidates for the development of polymer-based active fiber lasers or amplifiers near 1.06 and 1.3 μm.

Acknowledgements

The authors would like to thank Dr Paul Simon (Max Planck Institute for Chemical Physics of Solids, Dresden, Germany) for the TEM photomicrograph. We also thank M.Y. Yuce and M.N. Cizmeciyan for their assistance in measurements and preparation of figures. U. Demirbas acknowledges the support of the Scientific and Technical Research Council of Turkey (TUBITAK) in the framework of the BAYG program.

References

[1] Chen RT, Lee M, Natarajan S, Lin C, Ho ZZ, Robinson D. IEEE Photonic Technol L 1993;5(11):1328–31.
[2] Lin S, Feuerstein RJ, Mickelson AR. J Appl Phys 1996;79(6):2868–74.
[3] Kobayashi T, Nakatsuka S, Iwafuji T, Kuriki K, Imai N, Nakamoto T, et al. Appl Phys Lett 1997;71(17):2421–3.
[4] Koeppen C, Yamada S, Jiang G, Garito AF, Dalton LR. JOSA B 1997; 14(1):155–62.
[5] Zhang QJ, Wang P, Sun XF, Zhai Y, Dai P. Appl Phys Lett 1998;72(4): 407–9.
[6] Kuriki K, Kobayashi T, Imai N, Tamura T, Nishihara S, Tagaya A, et al. IEEE Photonic Technol L 2000;12(8):989–91.
[7] Yanagida S, Hasegawa Y, Wada Y. J Lumin 2000;87–89:995–8.
[8] Slooff LH, van Blaaderen A, Polman A, Hebbink GA, Klink SI, van Veggel FCJM, et al. J Appl Phys 2001;91(7):3955–80.
[9] Kuriki K, Nishihara S, Nishisawa Y, Tagaya A, Okamoto Y, Koike Y. Elect Lett 2001;37(7):415–7.
[10] Kuriki K, Koike Y, Okamoto Y. Chem Rev 2002;102:2347–56.
[11] Xu X. Opt Commun 2003;225:55–9.
[12] Hasegawa Y, Sogabe K, Wada Y, Yanagida S. J Lumin 2003;101:235–42.
[13] Hasegawa Y, Wada Y, Yanagida S. J Photochem Photobiol 2004;5: 183–202.
[14] Chen B, Dong N, Zhang Q, Yin M, Xu J, Liang H, et al. J Non-Cryst Solids 2004;341:53–9.
[15] Chen B, Xu J, Dong N, Liang H, Zhang Q, Yin M. Spectrochim Acta A 2004;60:3113–8.
[16] Zhang M, Lu P, Wang X, He L, Xia H, Zhang W, et al. J Phys Chem B 2004;108:13185–90.

[17] Kawa M, Frechet JMJ. Chem Mater 1998;10:286–96.
[18] Holder E, Marin V, Kozodaev D, Meier MAR, Lohmeijer BGG, Schubert US. Macromol Chem Phys 2005;206:989–97.
[19] Yilgor I, Sha'aban AK, Steckle WP, Tyagi D, Wilkers GL, McGrath JE. Polymer 1984;25(12):1800–6.
[20] Tyagi D, Yilgor I, McGrath JE, Wilkes GL. Polymer 1984;25(12): 1807–16.
[21] Yilgor E, Yilgor I. Polymer 2001;42(19):7953–9.
[22] Sheth JP, Aneja A, Wilkes GL, Yilgor E, Atilla GE, Yilgor I, et al. Polymer 2004;45(20):6919–32.
[23] Krevelen DWV. Properties of polymers: their correlation with chemical structure; their numerical estimation and prediction from additive group contributions. Amsterdam: Elsevier; 1990.
[24] Majumdar P, Webster DC. Macromolecules 2005;38(14):5857–9.
[25] Yilgor E, Gordeslioglu M, Dizman B, Yilgor I. In: Clarson JS, Fitzgerald JJ, Owen MJ, Smith SD, Dykes JV, editors. ACS symposium, vol. 838. Washington, DC: ACS; 2003.
[26] Keuleers R, Papaefstathiou GS, Raptopoulou CP, Tangoulis V, Desseyn HO, Perlepes SP. Inorg Chem Commun 1999;2:472–5.
[27] Bermudez VD, Ferreira RAS, Carlos LD, Molina C, Dahmouche K, Ribeiro SJL. J. Phys Chem B 2001;105:3378–86.
[28] Shen Q-D, Chen L, Hu T-D, Yang C-Z. Macromolecules 1999;32: 5878–83.
[29] Miniscalco WJ. Optical and electronic properties of rare earth ions in glasses. In: Digonet MJF, editor. Rare earth doped fiber lasers and amplifiers. New York: Marcel Dekker; 1993. p. 19–135.
[30] Kumar GA, Kaminskii AA, Ueda K-I, Yagi H, Yanagitani T, Unnikrishnan NV. IEEE J Quant Electron 2004;40(6):747–58.
[31] Judd BR. Phys Rev 1962;127(3):750–61.
[32] Ofelt GS. J Chem Phys 1962;37:511.
[33] Vleck JHV. J Phys Chem 1936;41:67.
[34] Broer LJF, Gorter CJ, Hoogschagen J. Physica 1945;11:231.
[35] Kaminskii AA. Crystalline lasers: physical processes and operating schemes. New York: CRC; 1996.
[36] Yatsimirskii KB, Davidenko NK. Coord Chem Rev 1979;27:223–73.
[37] Mehta PC, Tandon SP. J Chem Phys 1970;53:414.
[38] Carnall WT, Fields PR, Rajnak K. J Chem Phys 1968;49:4424.
[39] Mehta V, Aka G, Dawar AL, Mansingh A. Opt Mater 1999;12:53–63.
[40] Kaminskii AA, Boulon G, Buoncristiani M, Bartolo BD, Kornienko A, Mironov V. Phys Status Solidi 1994;141:471.
[41] Rao AS, Rao JL, Ahammed YN, Reddy RR, Rao TVR. Opt Mater 1998; 10:129–35.
[42] Krupke WF. IEEE J Quant Electron 1974;QE-10:450–7.
[43] Wachtler M, Speghini A, Gatterer K, Fritzer HP, Ajo D, Bettinelli M. J Am Ceram Soc 1998;81(8):2045–52.
[44] Kumar GA, Martinez A, Rosa EDL. J Lumin 2002;99:141–8.